PAPER • **OPEN ACCESS**

Dynamics of negative coronas in airflow

To cite this article: M Niknezhad *et al* 2021 *Plasma Sources Sci. Technol.* **30** 105001

OPEN ACCESS
IOP Publishing
Plasma Sources Science and Technology
Plasma Sources Sci. Technol. **30** (2021) 105001 (10pp)
https://doi.org/10.1088/1361-6595/ac24d2

Dynamics of negative coronas in airflow

M Niknezhad[1], O Chanrion[1,*], J Holbøll[2] and T Neubert[1]

[1] National Space Institute, Technical University of Denmark, Kongens Lyngby, Denmark
[2] DTU Elektro, Technical University of Denmark, Kongens Lyngby, Denmark

E-mail: chanrion@space.dtu.dk

Received 31 May 2021, revised 27 August 2021
Accepted for publication 8 September 2021
Published 7 October 2021

Abstract

Recent numerical studies captured the effects of airflow on positive streamers, when subjected to a lateral wind. The positive streamers initiate from the trailing side of the anode and propagate with a clear tilting in the direction of the airflow. In this paper, we present the results of a simulation of two successive negative corona pulses and investigate their behaviour when exposed to a lateral wind. We use a three-dimensional numerical model that couples the electrical discharge dynamics with the airflow and allows the study of the discharge on electrons and ions timescales. The results show that negative coronas are not easily influenced by the airflow and tilt just slightly in the flow direction. Our simulation explains the physical mechanism that governs the formation and termination of negative corona pulses (Trichel pulses) and describes for the first time the proposed cathode-directed streamer mechanism for negative corona current pulses.

Keywords: negative corona, Trichel pulses, gas discharges, extended model, airflow

(Some figures may appear in colour only in the online journal)

Introduction

In a recent paper [1], we discussed the effects of airflow on positive streamers to explain the experimental findings presented in [2] about electrical discharges under airflow. In this experiment, they observed that positive streamers tilt in the direction of the airflow while there were no significant effects on the negative corona. In [1], we modelled the effects of the airflow on positive streamers and confirmed the tilting of streamers in the direction of the wind. We found two mechanisms that elicit this behaviour. Firstly, the positive streamer channel remains attached to the surface of the anode although the wind tends to push off the particles away from the surface of the anode [1]. Secondly, the subsequent positive streamers emerge inside the previous channel and follow the pre-ionized path of the previous streamer [1].

In this paper, we model the effects of airflow on negative corona of type Trichel pulse [3], to explain the experimental findings presented in [2]. Trichel pulses refer to the intermittent corona pulsing first discovered by Trichel and Kip [4, 5]. We investigate if similar physical mechanisms observed for positive streamers in [1] are also observed for negative coronas and use a slightly modified version of the numerical model as described in [1]. It couples the extended drift-diffusion equations for charged particles, the Helmholtz equations for photoionization, the Poisson's equation for electric field, and the compressible Navier–Stokes equations for the airflow. The numerical model allows to study discharges at different timescales. Several authors have studied negative coronas using 1D and 2D axisymmetric models [6–13]. Our model is in 3D to take into account the lateral airflow. Negative corona simulations require a very fine mesh around the cathode due to the thin charge layer forming near the surface of the cathode, generally known as the cathode layer. The need of high spatial resolution appears extremely time consuming for long duration simulation of negative coronas. Our model uses unstructured grid, adaptive mesh refinement and an implicit solver, which allow a significant reduction of the computation time, making these simulations feasible.

In the first section we recall the numerical model and in the second section we present results from the simulation of two successive negative coronas exposed to a lateral wind. Finally, we show that our model captures the physical mechanisms

* Author to whom any correspondence should be addressed.

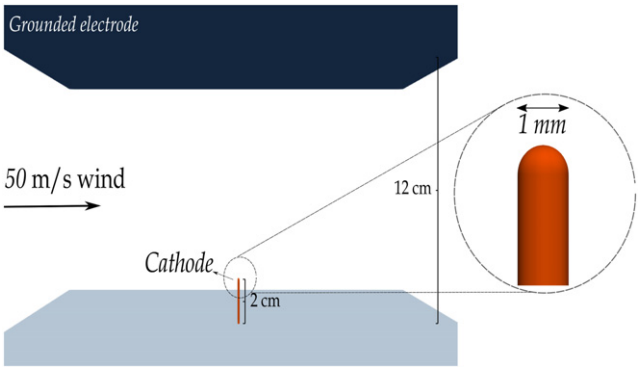

Figure 1. The discharge gap, where the cathode is at −10 kV potential.

behind the formation of Trichel negative pulses, specifically the streamer mechanism for negative corona current pulses (NCCPs) proposed in [3].

1. Physical model

The local density assumption commonly used along with the drift-diffusion model is not accurate for simulations with simultaneous presence of steep density gradients and high electric fields. For negative corona simulation, we expect that a region of high electric field and high charged particle density gradients forms near the surface of the cathode as previously reported in e.g. [3, 5, 8, 14].

Therefore, we modified our model [1] for a treatment of the drift-diffusion equations by the extended model described in [15–18]. This model relaxes the locality assumption in the calculation of the ionization source term and allows a more realistic estimation of the ionization source. We recall the extended model from [15], first the equation for the electrons reads:

$$\begin{aligned}\frac{\partial n_{\mathrm{e}}}{\partial t} &= \nabla\cdot(\boldsymbol{D}\ \nabla n_{\mathrm{e}}) + \nabla\cdot((\mu_{\mathrm{f}}\boldsymbol{E}+\boldsymbol{V}_{\mathrm{air}})n_{\mathrm{e}})\\ &\quad + n_{\mathrm{e}}(\nu_{\mathrm{i}}-\nu_{\mathrm{a}}) - (\boldsymbol{W}_{\mathrm{b}}-\boldsymbol{W}_{\mathrm{f}})\cdot\nabla n_{\mathrm{e}}\\ &\quad - S_{r_{\mathrm{e-p}}} + S_{\mathrm{ph}} \end{aligned} \tag{1.1}$$

,where n_{e} is the electron density and $\boldsymbol{E}$ is the electric field vector. $\boldsymbol{W_{\mathrm{f}}} = -\mu_{\mathrm{f}}\boldsymbol{E}$, $\boldsymbol{W_{\mathrm{b}}} = -\mu_{\mathrm{b}}\boldsymbol{E}$ and $\boldsymbol{D}$ are, respectively, the flux velocity vector, the bulk velocity vector and the flux diffusion coefficient. The electron bulk mobilities are evaluated using a particle model [19] and are in agreement with the values reported in [17]. μ_{f} is the flux mobility and ν_{i} and ν_{a} are the ionization and attachment rates all calculated using the Bolsig+ software, and depend solely on the local electric field [20–25]. The attachment rates are taken from [26] for electric fields below 40 Td, and are calculated using Bolsig+ [20] for higher electric fields. $S_{r_{\mathrm{e-p}}}$ is the electron–ion recombination term and is given by [26] and S_{ph} is the photoionization source term. As described in [1], we assume that the superposition law holds and approximate the velocities of particles in airflow by adding the air velocity $\boldsymbol{V}_{\mathrm{air}}$ to the particle drift velocity $\mu_{\mathrm{f}}\boldsymbol{E}$.

The equivalent ionization source term in (1.1) is given by:

$$S_{\mathrm{i}} = n_{\mathrm{e}}\nu_{\mathrm{i}} - (\boldsymbol{W}_{\mathrm{b}}-\boldsymbol{W}_{\mathrm{f}}).\nabla n_{\mathrm{e}}. \tag{1.2}$$

Similarly, the equation for the positive ions n_{p} reads:

$$\begin{aligned}\frac{\partial n_{\mathrm{p}}}{\partial t} &= \nabla\cdot(\boldsymbol{D}_{\mathrm{p}}\ \nabla n_{\mathrm{p}}) + \nabla\cdot((\mu_{\mathrm{p}}\boldsymbol{E}+\boldsymbol{V}_{\mathrm{air}})n_{\mathrm{p}})\\ &\quad + n_{\mathrm{e}}\nu_{\mathrm{i}} - (\boldsymbol{W}_{\mathrm{b}}-\boldsymbol{W}_{\mathrm{f}}).\nabla n_{\mathrm{e}}\\ &\quad - S_{r_{\mathrm{e-p}}} - S_{r_{\mathrm{n-p}}} + S_{\mathrm{ph}} \end{aligned} \tag{1.3}$$

and for the negative ions n_{n}:

$$\frac{\partial n_{\mathrm{n}}}{\partial t} = \nabla\cdot(\boldsymbol{D}_{\mathrm{n}}\ \nabla n_{\mathrm{n}}) + \nabla\cdot((\mu_{\mathrm{n}}\boldsymbol{E}+\boldsymbol{V}_{\mathrm{air}})n_{\mathrm{n}}) + n_{\mathrm{e}}\nu_{\mathrm{a}} - S_{r_{\mathrm{n-p}}}, \tag{1.4}$$

where $S_{r_{\mathrm{n-p}}}$ is the ion–ion recombination loss term given by [26]. The ions transport coefficients are given by [27, 28]. We have modelled the photoionization source term S_{ph} in (1.1) and (1.3) using the approximation proposed by [29], which is calculated based on the set of three Helmholtz differential equations, also described in [30]. Further details regarding the description of the photoionization in our numerical model is provided in [1].

2. Simulations

The simulations are done in a discharge gap where the point cathode with a tip radius of 0.5 mm is at −10 kV and is exposed to a 50 m s^{-1} lateral wind, see figure 1. A neutral plasma patch of maximum density 10^{18} m^{-3} and an e-folding radius of 0.5 mm is placed on the cathode tip to facilitate the streamer formation.

The minimum mesh size around the cathode is 0.2 μm normal to the cathode surface, allowing to have a fine mesh to resolve the sharp density variations as shown in [8]. To counter the impact of the fine mesh size on the computation time, we use the implicit-ELP integration scheme proposed in [31]. It integrates the ionization and attachment part of electrons/ions dynamics in an exact manner, and relaxes the constraints on the time step size imposed by the Courant–Friedrich–Lewi stability condition and the restriction of the time step due to dielectric relaxation time [32]. Therefore, as we have previously shown in [1], long time steps can be used with minimal inaccuracies. In our simulation, the time step varies between 1 ps during the pulse to 2 nanoseconds between the pulses when the field and the density variations slow down.

Ion-impact electron emission is implemented in this simulation, which models the release of electrons by the incident positive ions at the cathode. We used an ion-impact emission coefficient of 0.005 in agreement with the range reported in [6, 8, 14].

The airflow field is calculated using the compressible Navier Stokes equations and the $k-\omega$ turbulence model [33], similar to our previous study for positive streamers in [1]. The air streamlines are shown in figure 2.

In the following, we present the results from the simulation of two successive negative coronas.

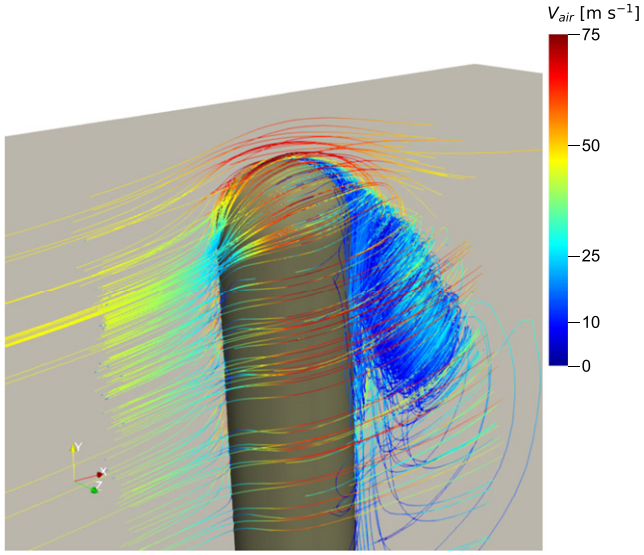

Figure 2. The airflow streamlines around the cathode with a diameter of 1 mm. The air pressure and temperature at inlet are respectively 1 bar and 300 K.

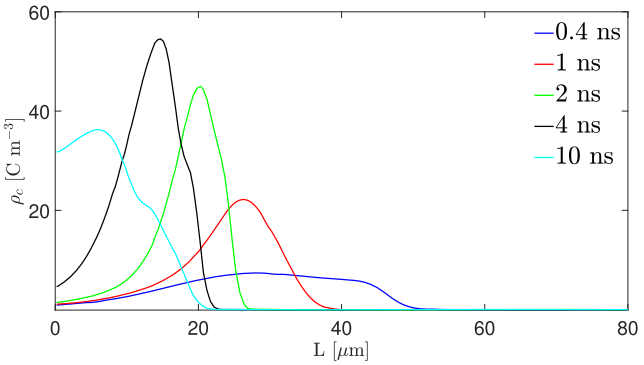

Figure 3. Charge density profiles along the cathode axis during the initial corona pulse at 0.4, 1, 2, 4, and 10 ns.

2.1. Initial corona pulse

The first corona pulse initiates as the potential is applied to the cathode, leading to the formation of a sharp positive charge layer over the surface of the cathode that propagates toward the cathode, as shown by the charge density profiles in figure 3. This well known phenomena has been previously described in [3, 5, 6, 8, 34], where a positive charge layer forms near the surface of the cathode with significant electric field intensification in a narrow region close to the cathode surface.

Figure 4 shows the electric field, electron density and positive and negative ion densities at 2, 50, and 200 ns. As the positive charge layer, shown in figure 3, gets closer to the cathode, a region of very high electric field forms between the charge layer and the cathode, see figure 4 (1st row). The narrow cathode sheath with positive charges is formed a few tens of μm above the cathode surface and enhances the field in the cathode layer, while the field is screened inside the negative corona. The very high electric field in the cathode layer has been previously estimated from experimental data in [5] and observed numerically in [8].

The positive charge layer slowly moves toward the cathode, see figure 3, increasing the maximum electric field while narrowing down the high electric field region. As the width of the high electric field region becomes smaller, the length available for electrons to multiply gets limited. Therefore, as the positive ions of the charge layer get absorbed by the cathode there would not be enough ionization to replenish the positive charge layer, which results in the gradual removal of the charge layer that can be seen in figure 3 at 10 ns.

The electric field inside the negative corona is low due to the screening effect of the positive charge layer, shown in figure 4 (1st row). In this zone, the three-body attachment plays a major role on the mobility of negative charge carriers since the reaction combines electrons and neutral gas molecules to form slow negative ions, see figure 4 (last row). As the positive charge layer disappears these slow negative ions screen the field around the cathode inhibiting the formation of a new pulse. It takes a long time for the negative ions to move away from the vicinity of the cathode and hence a long inter-pulse time, as previously pointed out in [6]. The small length scale of the sheath layer and the narrow high electric field cathode layer confirms the choice of the extended model which results in a more accurate fluid description.

2.2. Quiescent phase

The quiescent phase appears after the initial corona pulse and it continues till 35 μs when the 2nd corona pulse appears. The evolution of the quiescent phase is shown in figure 5 at 1, 10 and 20 μs.

During the quiescent phase the negative ions formed during the first corona pulse drift away from the cathode, leading to a sustained increase of the electric field near the cathode surface, as shown in figure 5 (1st and last rows). Similarly, we can see the gradual increase of the maximum electric field in figure 6, where we show the temporal evolution of the maximum electric field.

The effect of the airflow is evident in figure 5 (2nd and 3rd rows), which show the displacement of the electrons and positive ions during the quiescent phase due to the airflow. The densities of the charged particles left by the 1st corona pulse decrease while being moved by the air. The main mechanism removing the electrons is attachment, the positive ions are removed due to the absorption by the cathode and the recombination with the negative ions. One can note that the density of positive and negative ions are about 4 orders of magnitude larger than electrons, which is due to the smaller time constant of attachment mechanism compared to other involved mechanisms.

In our previous paper [1], we investigated the positive streamers in lateral airflow and we showed that the electrons from the previous positive streamer channel move toward the anode, ionizing the gas in the high electric field region around the anode. For negative polarity, electrons from the plasma sheath are pushed away from the cathode and are lost by strong attachment. Consequently, they do not contribute to the

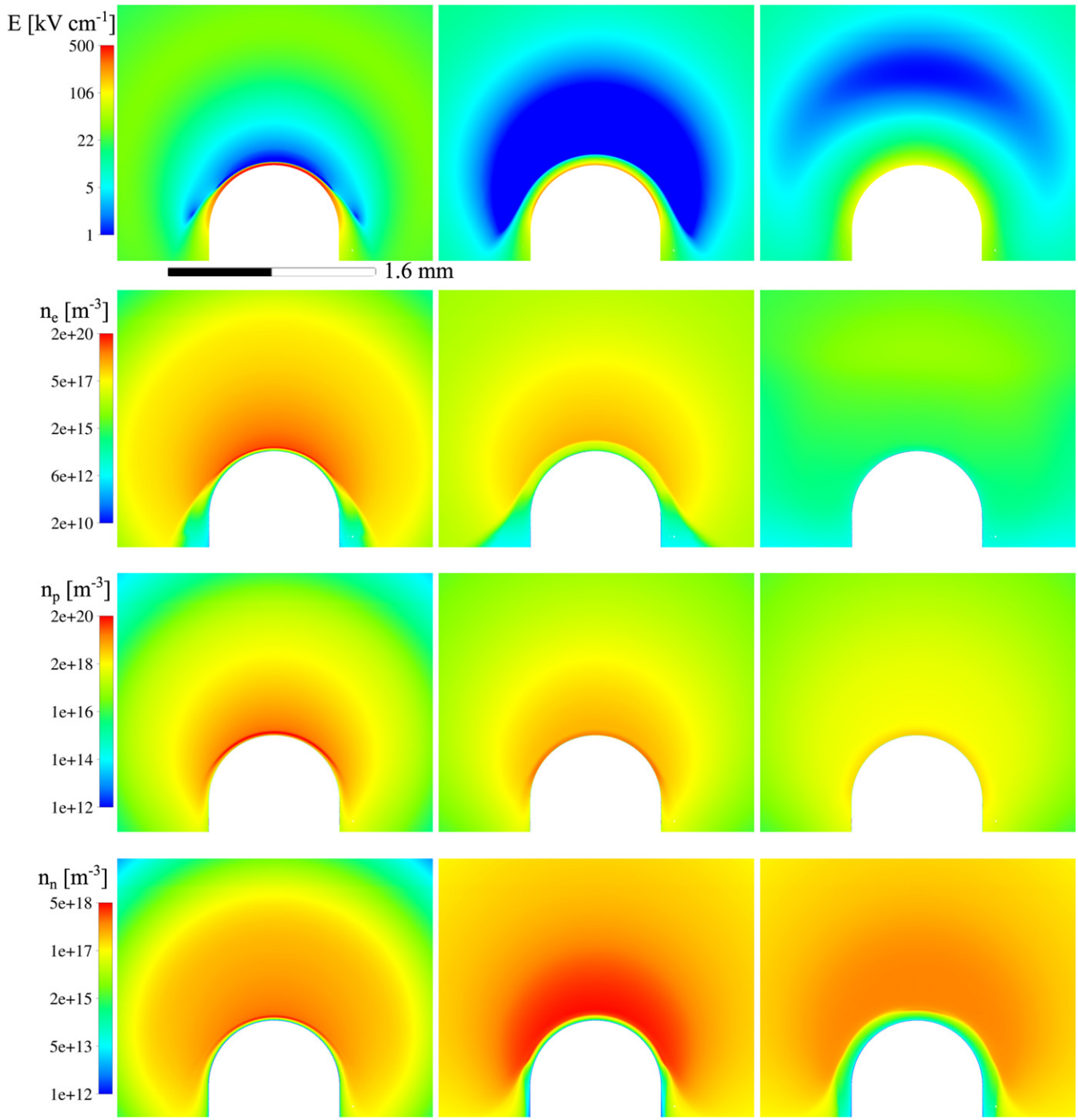

Figure 4. Contour plots of the electric field, electron density and positive and negative ions around the cathode tip during the initial corona pulse at 2 ns (left), 50 ns (center) and 200 ns (right).

electron production near the cathode surface. The densities of the electrons and positive ions remaining from the initial corona pulse near the cathode surface decline, and hence do not play a role in the formation of the 2nd corona pulse. Therefore, the mechanism observed for positive streamers and presented in [1] does not exist for negative coronas.

As the cathode electric field gradually returns back to the Laplacian field, the electron and positive ion densities start to build up just above the cathode tip. The increase in the electron and positive ion densities start gradually from around 30 μs and continues over the next 5 μs until the formation of a new negative corona pulse.

The evolution of the electron and positive ions densities before the onset of the second corona pulse is presented in figure 7 at 30, 33, and 34 μs. We can see that while the electron and ions densities are increasing, they are shifting in the direction of the wind. The displacement of this growing charged particle densities by the airflow is small as compared to the

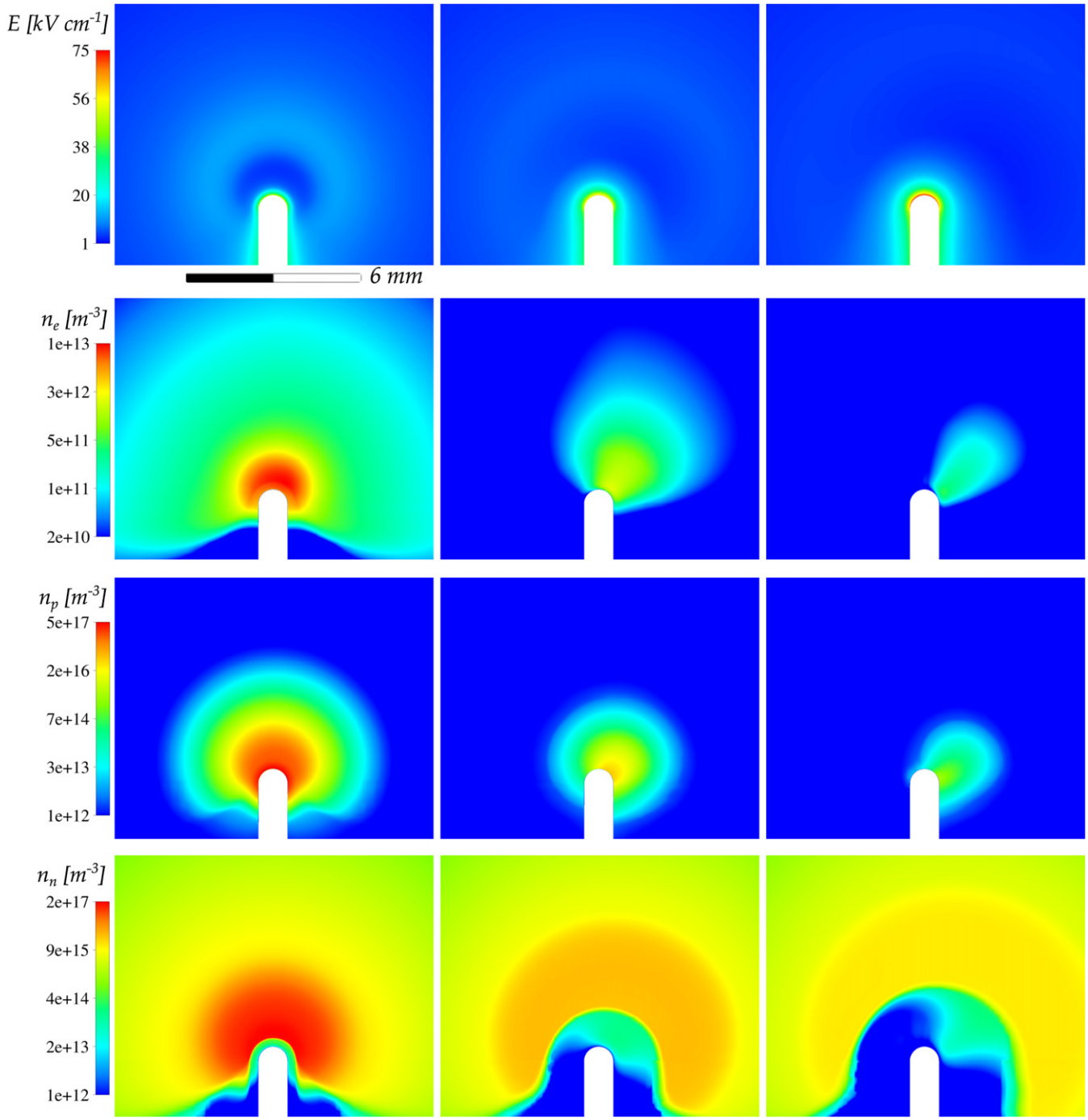

Figure 5. Contour plots of the electric field, electron density and positive and negative ion densities around the cathode tip during the quiescent phase at 1 μs (left), 10 μs (center) and 20 μs (right).

displacement of the remaining particles of the 1st corona because of its shorter exposure to the wind. In figure 7, we can also observe that the electron and positive ion densities left by the previous negative corona has decreased to a level negligible as compared to the electron and ion densities building up close to the cathode axis. This explains why the second negative corona pulse starts almost on the axis and is poorly influenced by the wind. It is now clear that the effects of the wind on negative coronas are not as notable as the effects on positive streamers previously observed in [1].

This result is in agreement with the experiment of [2] that did not observe any significant shifting of the negative corona with a wind speed of 20 m s^{-1}. Our simulation do not observe either with a wind speed of 50 m s^{-1}.

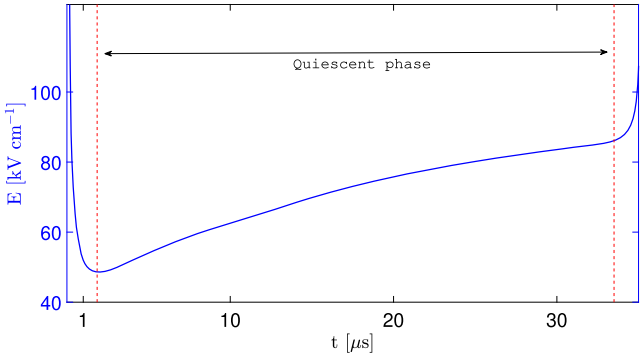

Figure 6. Evolution of the maximum electric field during the quiescent phase.

2.3. 2nd corona pulse

Although the formation of the second negative corona pulse is expected to be poorly influenced by the wind, we present in this section details of the formation of the second corona pulse, since our model reproduces the mechanisms proposed in [3] based on experiments. In [3], it was hypothesized that the behaviour of the NCCP can be explained by the formation of a cathode-directed streamer propagating toward the cathode.

From our simulation, we observe at about 35 μs that the density of the plasma above the surface of the cathode grows to a level that creates space charge fields comparable to that of the cathode which leads to the initiation of a cathode-directed streamer. The evolutions of the electric field and electron density are shown in figures 8 and 9 from 50 to 100 ns after 35 μs. The figures illustrate the formation of the cathode-directed streamer by showing the increase of the electric field and the electron density as the cathode-directed streamer propagates toward the cathode.

As the streamer approaches the cathode, the high electric field region at the streamer tip is limited by the cathode and becomes too small to provide enough electron multiplication and the propagation of the streamer tip slows down. The slowing down of the cathode-directed streamer can be seen in figure 10, which shows the propagation velocity of the streamer tip toward the cathode and the discharge current. The current is calculated following the energy conservation from [35]. In figure 10, the fast propagation of the cathode-directed streamer correlates well with the initially sharp rate of increase of the discharge current. As the streamer propagation toward the cathode surface slows down, electron multiplication continues on the sides of the streamer sustaining the enlarging and flattening of the streamer head on the cathode. The streamer charge layer propagates laterally on the surface and basically becomes the cathode layer slowly covering the cathode surface. After the initial fast propagation of the streamer, the movement of the positive charge layer toward the cathode relies mainly on the motion of the positive ions, as seen by the low velocity of the streamer toward the cathode in figure 10.

The movement of the positive ions toward the cathode results in a narrower cathode layer with higher electric field. The narrow cathode layer limits the electron multiplication and hence the positive charge layer cannot replenish its density compensating for the positive charges absorbed by the cathode. This results in continuous depletion of the positive charge layer and hence the drop in the cathode layer electric field.

Figure 11 shows the evolution of the discharge current and of the maximum electric field, the streamer onset is indicated by the dashed vertical line. From the figure, we can see that the current and electric field increase slowly till 80 ns after 35 μs, in this regime the multiplication of charges in the electron cloud above the surface of the cathode follows the Townsend discharge mechanism. As the charge induced electric field becomes comparable to the background field, the discharge regime changes and becomes a cathode-directed positive streamer which drives the charge production mechanism. This leads to the fast increase in the discharge current along with the sharp rise of the electric field seen on figure 11. The discharge current reaches its maximum as the positive charge layer reaches the surface of the cathode and the electric field maximizes. As the positive charge layer and the electric field in the cathode layer decreases, the discharge current experiences a sustained decreasing profile which continues to decline till the next negative pulse.

The sharp decrease in the electric field and consequently in the discharge current seen in figure 11, is due to the absorption of the positive charge layer ions by the cathode and the field screening by the negative ions. However, the contribution of the negative ions on the initial drop of the electric field is relatively small. We have calculated the maximum field in the cathode layer with and without the influence of negative ions and defined the following variable as a measure of the influence of the negative ions in the maximum field:

$$R = 1 - \frac{\text{Maximum field}}{\text{Maximum field without negative ions}}. \qquad (2.1)$$

We have plotted the value of R as a function of time in figure 12 along with the current. We can see that at around 92 ns after 35 μs where the current is at its maximum the field screening effect of the negative ions is relatively small and the main mechanism behind the drop in the electric field and the current is the absorption of the positive ions by the cathode. Later, as the negative ions density rises, the influence of negative ions on field screening becomes the major mechanism behind the decrease in the current, see figure 12. This result suggests that the presence of negative ions is not essential for the termination of the pulse and hence the Trichel negative corona pulses can theoretically occur in both electronegative and electropositive gasses as previously shown experimentally by [34, 36, 37].

3. Conclusion

In an earlier paper [1], we explained the effects of the transversal airflow on positive streamer discharges which came essentially from the redistribution of the charged particles left by a previous streamer. We showed that the lateral airflow shifted the charged particles on the anode surface leading to a tendency of subsequent streamers to initiate and propagate toward

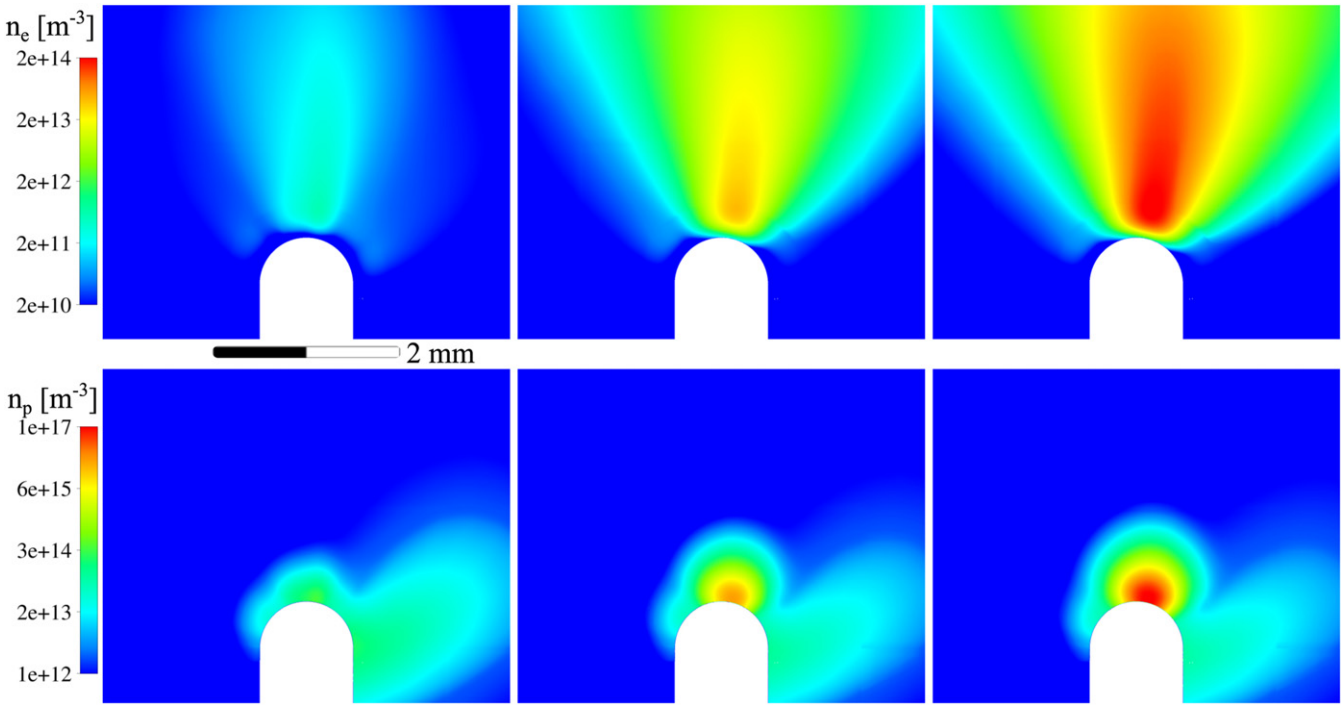

Figure 7. Contour plots of electrons and positive ions densities at 30 μs (left), 33 μs (center) and 34 μs (right), prior to the onset of the 2nd corona pulse.

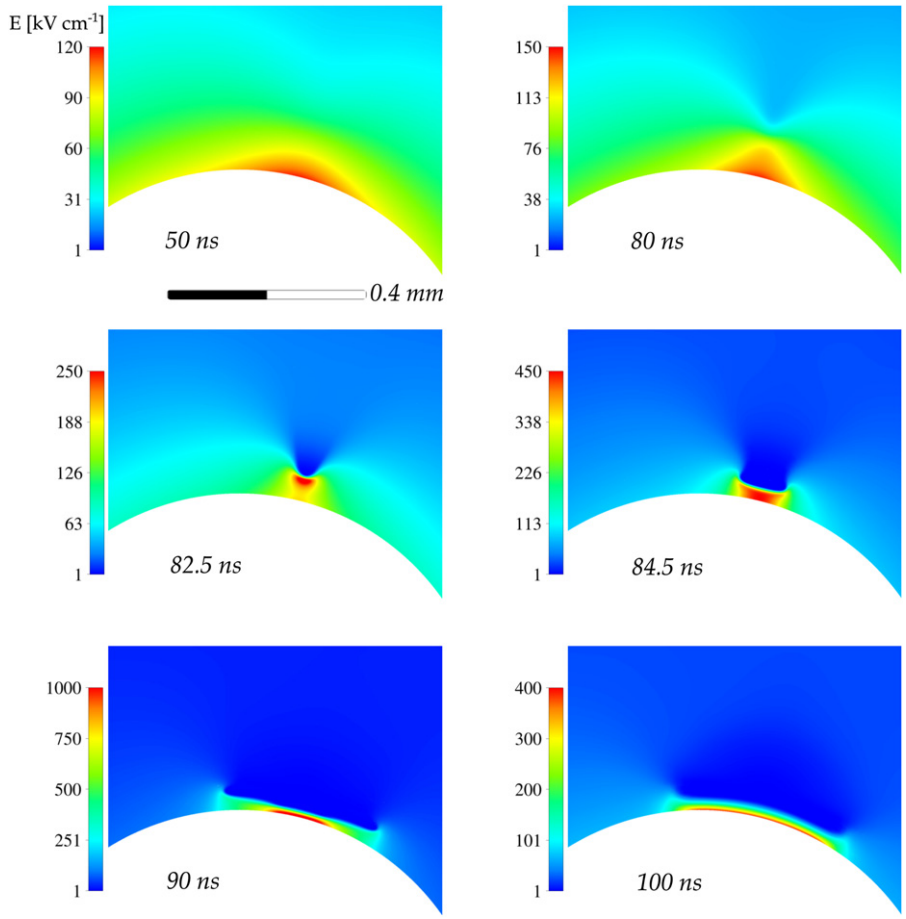

Figure 8. Electric field contours during the initiation, propagation and termination of the cathode-directed streamer, the time is given as the number of nanoseconds after 35 μs.

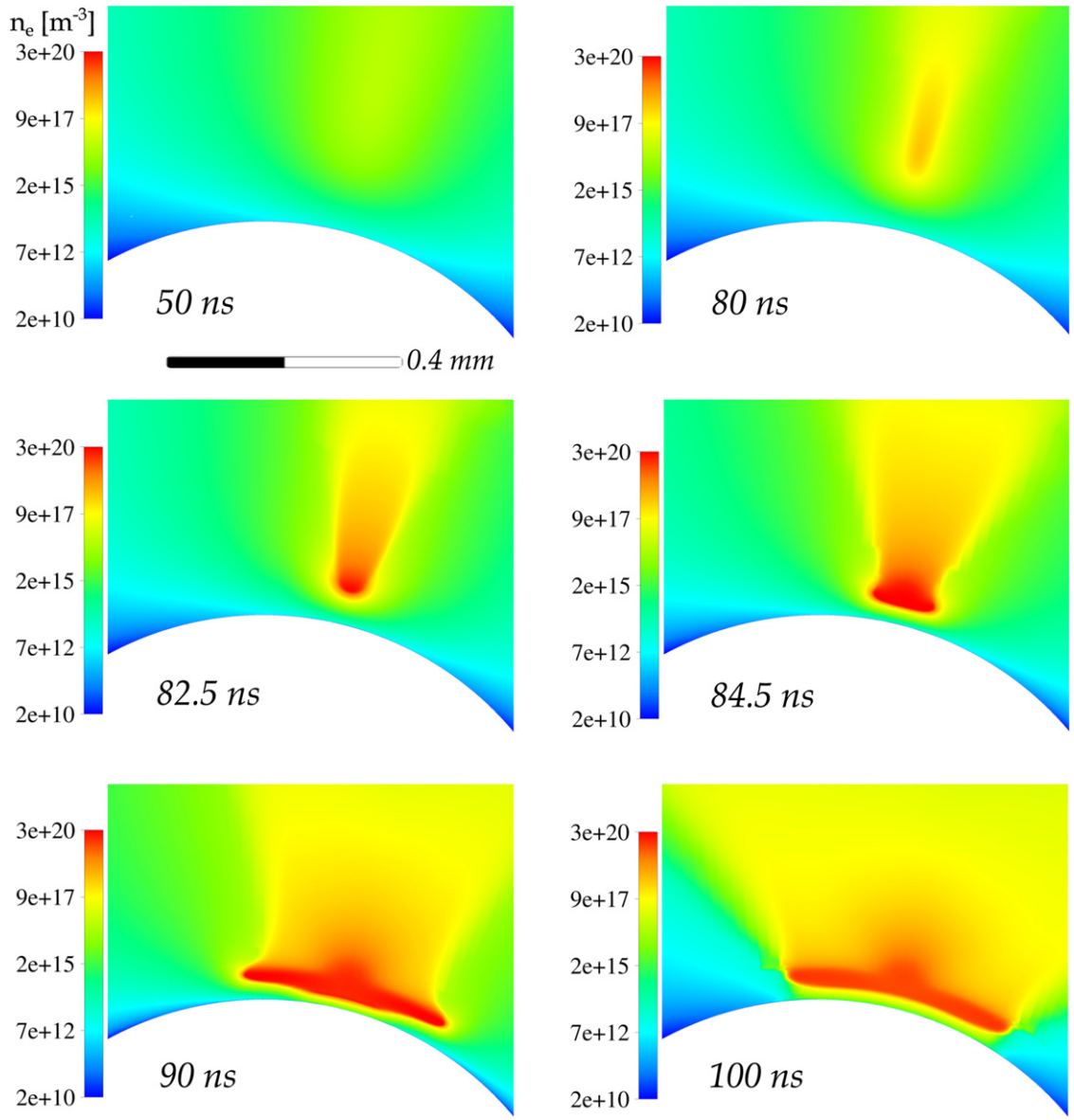

Figure 9. Electron density contours during the initiation, propagation and termination of the cathode-directed streamer, the time is given as the number of nanoseconds after 35 μs.

the trailing edge of the anode. The charges were maintained on the surface since the electrons from previous positive streamer channel move toward the anode and ionize the gas at the high electric field region. We showed that this mechanism leads to a significant tilting of subsequent positive streamers in the direction of the airflow. In this paper, we investigate the dynamics of negative coronas in airflow. We used a highly accurate 3D model and performed a simulation of negative coronas exposed to a lateral wind. We report on the influence of the airflow on two successive corona pulses emerging from the cathode and conclude that the mechanism explaining the displacement of positive streamers does not exists for the streamers of negative polarity. The main reason originates from the fact that the electrons in the negative plasma sheath are pushed away from the cathode toward the low field region and are lost to strong attachment. Therefore, the densities of electrons and positive ions remaining from the 1st corona pulse are significantly reduced while being moved by the airflow and do not play a role in the formation of the subsequent negative corona pulse. The 2nd corona pulse forms in the vicinity of the cathode axis. The slight displacement of the 2nd corona from the cathode axis is due to the shifting of the electrons and positive ions at the timescale of the formation of the cathode-directed streamer.

Similar to the modelling results that we obtained for positive streamers in [1], our present results are in good agreement with the experimental results previously reported by [2]. Furthermore, we showed that our model is to our knowledge one of the first 3D streamer models to capture the main mechanisms involved in the formation of Trichel corona pulses, in particular it describes the cathode-directed streamer mechanism for NCCPs, experimentally evidenced in [3]. We observe that the

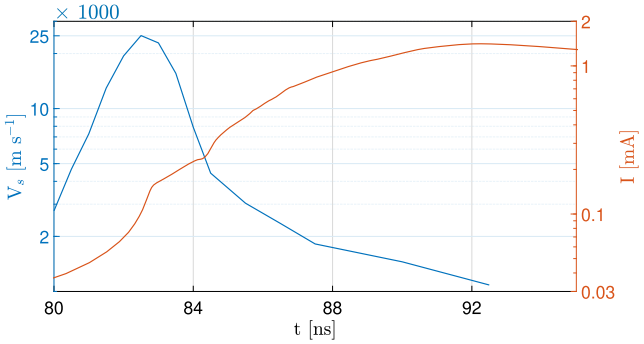

Figure 10. Cathode-directed streamer propagation velocity toward the cathode and the discharge current (log scale), the time is given as the number of nanoseconds after 35 μs. The dashed vertical line marks the time when the positive streamer charge layer starts to flatten and transversally propagates over the cathode surface (see figures 8 and 9).

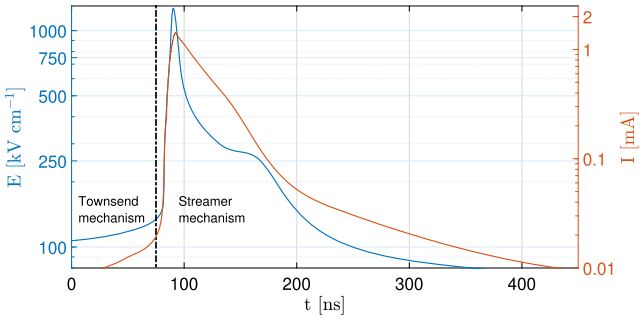

Figure 11. Evolution of the electric field and the discharge current (log scale) over the duration of the 2nd negative corona pulse, the time is given as the number of nanoseconds after 35 μs. The dashed vertical line shows the onset of the cathode-directed streamer.

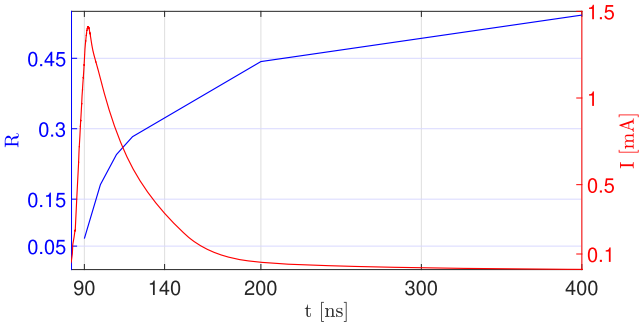

Figure 12. Variable R and the discharge current as a function of time given as the number of nanoseconds after 35 μs.

Trichel pulse is associated with the formation and propagation of a positive streamer toward the cathode surface.

We showed that the current waveform correlates well with the evolution of the positive streamer describing the different stages of the current pulse. The Townsend regime corresponds to the formation, the rise time corresponds to the initiation and propagation and the final decay corresponds to the termination of the cathode-directed streamer.

The results also illustrate that the fast decay of the Trichel pulse is due to a prior absorption of the positive charge layer by the cathode which is followed by the screening of the field by negative ions. This finding supports that the Trichel pulses can theoretically occur also in electropositive gasses [34, 36, 37].

Acknowledgments

This project has received funding from the European Unions Horizon 2020 research and innovation programme under the Marie Sklodowska-Curie Grant Agreement No. 722337. The computational resources were provided by DTU Computing Center (DCC).

Data availability statement

The data that support the findings of this study are available upon reasonable request from the authors.

ORCID iDs

M Niknezhad https://orcid.org/0000-0003-0748-2586
O Chanrion https://orcid.org/0000-0002-4484-4104
J Holbøll https://orcid.org/0000-0001-7578-8304
T Neubert https://orcid.org/0000-0001-7851-7788

References

[1] Niknezhad M, Chanrion O, Köhn C, Holbøll J and Neubert T 2021 *Plasma Sources Sci. Technol.* **30** 045012
[2] Vogel S and Holboll J 2018 *IEEE Trans. Dielectr. Electr. Insul.* **25** 721–8
[3] Černák M, Hosokawa T, Kobayashi S and Kaneda T 1998 *J. Appl. Phys.* **83** 5678–90
[4] Trichel G W 1938 *Phys. Rev.* **54** 1078–84
[5] Raizer Y P, Kisin V I and Allen J E 1991 *Gas Discharge Physics* (Berlin: Springer)
[6] Morrow R 1985 *Phys. Rev.* A **32** 1799–809
[7] Reess T and Paillol J 1997 *J. Phys. D: Appl. Phys.* **30** 3115–22
[8] Tran T N, Golosnoy I O, Lewin P L and Georghiou G E 2010 *J. Phys. D: Appl. Phys.* **44** 015203
[9] Gupta D K, Mahajan S and John P I 2000 *J. Phys. D: Appl. Phys.* **33** 681–91
[10] Napartovich A P, Akishev Y S, Deryugin A A, Kochetov I V, Pan'kin M V and Trushkin N I 1997 *J. Phys. D: Appl. Phys.* **30** 2726–36
[11] Sattari P, Castle G S P and Adamiak K 2011 *IEEE Trans. Ind. Appl.* **47** 1935–43
[12] Dordizadeh P, Adamiak K and Castle G S P 2015 *J. Phys. D: Appl. Phys.* **48** 415203
[13] Chen S, Li K and Nijdam S 2019 *Plasma Sources Sci. Technol.* **28** 055017
[14] Soria-Hoyo C, Pontiga F and Castellanos A 2007 *J. Phys. D: Appl. Phys.* **40** 4552–60
[15] Petrović Z L, Dujko S, Marić D, Malović G, Nikitović Ž, Šašić O, Jovanović J, Stojanović V and Radmilović-Raenović M 2009 *J. Phys. D: Appl. Phys.* **42** 194002
[16] Li C, Ebert U and Hundsdorfer W 2010 *J. Comput. Phys.* **229** 200–20
[17] Li C, Ebert U and Hundsdorfer W 2012 *J. Comput. Phys.* **231** 1020–50
[18] Aleksandrov N L and Kochetov I V 1996 *J. Phys. D: Appl. Phys.* **29** 1476–83

[19] Chanrion O and Neubert T 2008 *J. Comput. Phys.* **227** 7222–45
[20] Hagelaar G J M and Pitchford L C 2005 *Plasma Sources Sci. Technol.* **14** 722–33
[21] Lawton S A and Phelps A V 1978 *J. Chem. Phys.* **69** 1055–68
[22] Yamabe C, Buckman S J and Phelps A V 1983 *Phys. Rev.* A **27** 1345–52
[23] Phelps A V and Pitchford L C 1985 *Phys. Rev.* A **31** 2932–49
[24] Lawton S A and Phelps A V PHELPS database http://lxcat.laplace.univ-tlse.fr retrieved 4 June 2013
[25] Phelps A V and Pitchford L C SIGLO database http://lxcat.laplace.univ-tlse.fr (retrieved 4 June 2013)
[26] Pancheshnyi S, Nudnova M and Starikovskiy A 2005 *Phys. Rev.* E **71** 016407
[27] Ellis H W, Pai R Y, McDaniel E W, Mason E A and Viehland L A 1976 *At. Data Nucl. Data Tables* **17** 177–210
[28] Viehland L A and Kirkpatrick C C 1995 *Int. J. Mass Spectrom. Ion Process.* **149–150** 555–71
[29] Luque A, Ebert U, Montijn C and Hundsdorfer W 2007 *Appl. Phys. Lett.* **90** 081501
[30] Bourdon A, Pasko V P, Liu N Y, Célestin S, Ségur P and Marode E 2007 *Plasma Sources Sci. Technol.* **16** 656–78
[31] Beylkin G, Keiser J M and Vozovoi L 1998 *J. Comput. Phys.* **147** 362–87
[32] Hagelaar G J M and Kroesen G M W 2000 *J. Comput. Phys.* **159** 1–12
[33] Menter F 1993 Zonal two equation *k-w* turbulence models for aerodynamic flows *23rd Fluid Dynamics, Plasmadynamics, and Lasers Conf.*
[34] Zhang Y, Xia Q, Jiang Z and Ouyang J 2017 *Sci. Rep.* **7** 10135
[35] Morrow R and Sato N 1999 *J. Phys. D: Appl. Phys.* **32** L20L22
[36] Černák M and Hosokawa T 1988 *Appl. Phys. Lett.* **52** 185–7
[37] Akishev Y S, Grushin M E, Karal'nik V B and Trushkin N I 2001 *Plasma Phys. Rep.* **27** 520–31